Adsorption Kinetics of Light Paraffins in AC by a Constant Molar Flow-Rate Method

I. Prasetyo and D. D. Do
Dept. of Chemical Engineering, University of Queensland, Brisbane, QLD 4072, Australia

A semibatch constant molar flow-rate technique developed earlier by Do was applied to a series of light paraffins adsorbing onto a number of adsorbents. The adsorption and diffusion of methane, ethane, propane and n-butane on activated carbon at different temperatures were studied to determine the diffusivity of surface diffusion and its activation energy. It was found that the surface diffusivity decreases with the molecular weight in an exponential manner and increases with temperature according to the Arrhenius law. The ratio of the activation energy for surface diffusion to the heat of adsorption increases with the carbon number. A mechanism for surface diffusion is suggested to explain this increase.

Introduction

The way that a kinetic experiment is carried out is important in the determination of the kinetic parameters. For example, in the breakthrough curve experiment, the adsorbate is introduced by passing a constant flow of adsorbate through the bed, and the system response is monitored through the breakthrough curve, which is then analyzed to determine the kinetic parameters within the particle. Since this response is masked by many other processes, such as axial dispersion in the bed, the determination of intraparticle kinetic parameters is not very reliable. Another example is the use of TGA where the flow into the bed is constrained by the low flow into the microbalance so that the balance is not hydrodynamically disturbed. Realizing the difficulties of many methods, Do (1995) first proposed a method called the constant molar flow technique (CMF), and recently this technique was experimentally tested and validated with methane and carbon dioxide adsorption onto activated carbon (Prasetyo and Do, 1998). The activation energy for surface diffusion of carbon dioxide was found to agree well with the theoretical value obtained by Rao et al. (1985).

Basically in this method, a constant flow of pure adsorbate is introduced into a semibatch adsorber in which a small amount of adsorbents is accommodated. The supply of adsorbate is introduced slowly to avoid any abrupt heat release traditionally encountered in other methods, such as the batch adsorber or the TGA. In these techniques, the initial rate of adsorption is large enough to cause a high heat release, resulting in a significant temperature change within the particle, which would make the physical interpretation and the analysis more difficult. If such a heat transfer is not correctly accounted for, the kinetic parameters extracted for mass transfer will be erroneous. This disadvantage was eliminated in our technique, where the isothermal conditions are almost always ensured due to the slow introduction of the adsorbate. Another advantage of the CMF method is the short time required to obtain a kinetic curve, compared to a large amount of time needed in the DAB method (Do et al., 1991).

The objective of the present study was to extend the CMF method developed in our previous study to stronger adsorbing gases and investigate the surface diffusion of these gases.

Experimental Studies

The activated carbon used in this study was Ajax Activated Carbon (AC) Type 976 [1/16-in. (1.6-mm) cylindrical pellets], supplied by Ajax Chemicals-Australia; the physical properties of this carbon are listed in Table 1 (Gray and Do, 1991). Three different sizes of slab-shaped adsorbent particles (length: 0.5, 0.75, and 1.0 cm) and several adsorption temperatures were studied to explore their effects on the adsorption rate. Slab-shaped activated carbon particles were prepared

Correspondence concerning this article should be addressed to D. D. Do.

Table 1. Physical Properties of Ajax Activated-Carbon Adsorbent

Bulk (apparent) density	0.66 g/cm^3
Particle density	0.733 g/cm^3
Total porosity	0.71
Micropore (< 5.0 nm) porosity	0.40
Macropore (> 5.0 nm) porosity	0.31
Average macropore diameter	0.8 μm
BET (N_2) surface area	1,200 m^2/g

by coating their cylindrical surface with high-strength epoxy resin so that mass transfer can occur only through the flat surfaces (that is, one-dimensional diffusion in rectangular coordinates). All gases used in this experiment were of high purity unless otherwise stated, and they were obtained from the BOC Gases-Australia. The water-vapor impurity was removed by a bed containing molecular sieves 4A [1/8-in. (3.2-mm) pellets].

The adsorption-rate measurements were carried out with a semibatch adsorber, and the details of the experimental procedure were described in our previous study (Prasetyo and Do, 1998). The apparatus (Figure 1) essentially consists of two sections, the reservoir and adsorption sections, separated by a variable leak valve (Varian Model 951-5106), which accurately controls the low flow of adsorbate from the reservoir section to the adsorption section. Prior to each run, the sample was degassed at 150°C overnight until the pressure in the system was at least 10^{-5} torr. At $t = 0^+$, a constant molar flow of adsorbate from the reservoir was introduced slowly into the adsorption cell. The pressure of the adsorption cell was monitored by a Baratron pressure transducer and logged into a PC. The volume of the semibatch adsorber is 70.5 cm^3.

The run was terminated before the equilibrium between the two phases violated the Henry law condition. After completing one run, the sample was then cleaned and ready for another run at a different molar flow rate. For each adsorption temperature, three different molar flow rates were used.

To analyze the experimental data collected in this article, we used an analysis done by Do (1995). In this model, the mass transfer is assumed to be controlled by the dual flow of adsorbate into the interior of the particle. One flow is the pore volume diffusion, while the other is the diffusion of the adsorbed species. For this mechanism, the mass-balance equation describing the adsorbate distribution within the particle is

$$\epsilon_m \frac{\partial C}{\partial t} + (1-\epsilon_m)\frac{\partial C_\mu}{\partial t} = \epsilon_m D_p \frac{1}{r^s}\frac{\partial}{\partial r}\left(r^s \frac{\partial C}{\partial r}\right) + (1-\epsilon_m) D_s \frac{1}{r^s}\frac{\partial}{\partial r}\left(r^s \frac{\partial C_\mu}{\partial r}\right). \quad (1)$$

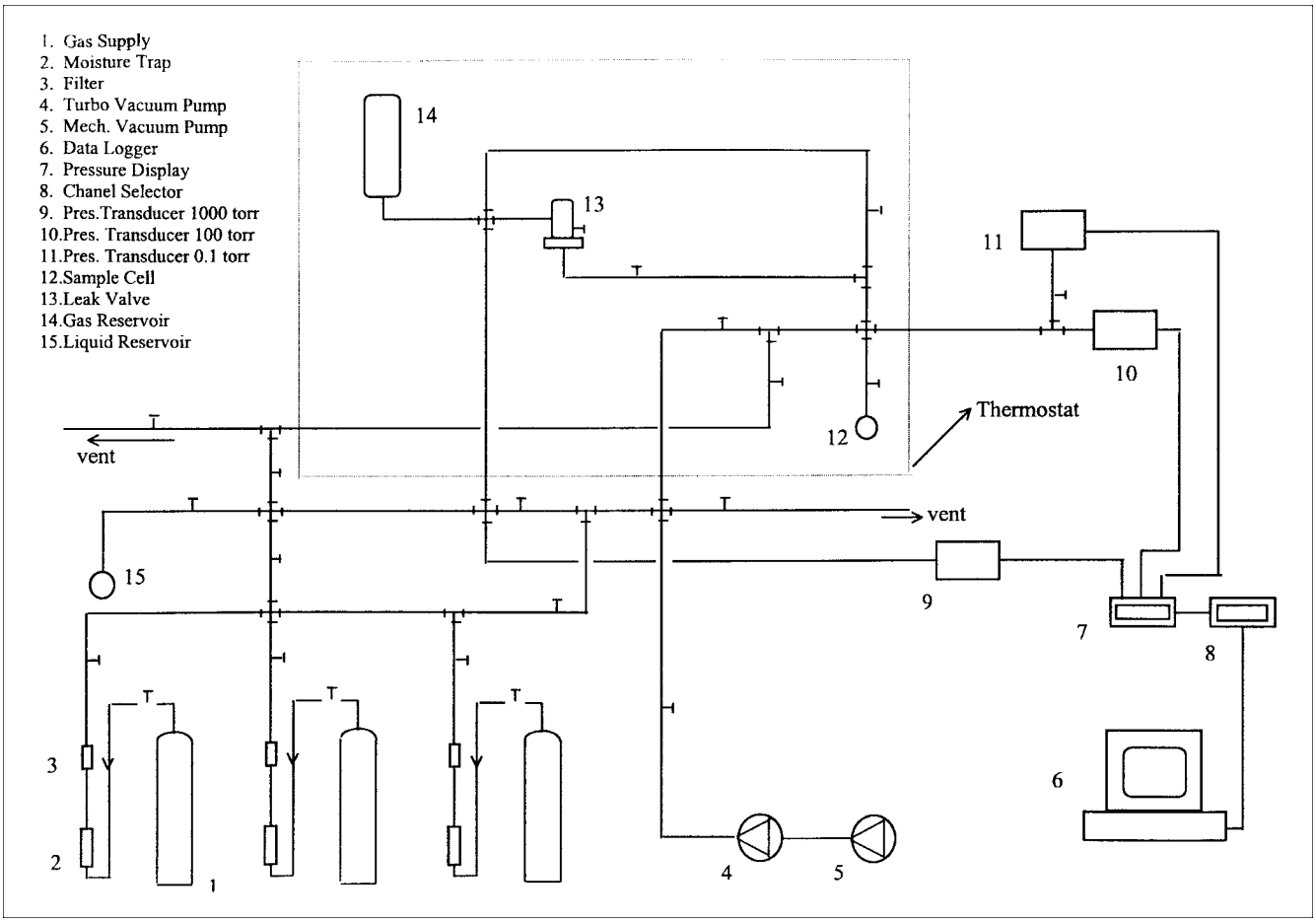

Figure 1. Experimental installation for dynamic (semibatch constant molar flow rate) measurements.

Carrying out the mass balance of the adsorption system yields

$$\dot{N} = V\frac{\partial C}{\partial t} + V_\mu \frac{\partial C_\mu}{\partial t}, \tag{2}$$

where $\dot{N}$ (gmol/s) is the molar supply rate of the adsorbate into the adsorption cell and has a free volume of V; C is the adsorbate concentration in the gas phase; and C_μ is the adsorbate concentration in the solid phase, defined as mole per unit volume of the adsorbed phase.

Solving the particle mass-balance equation (Eq. 1) with the overall mass-balance equation around the adsorber (Eq. 2) and assuming a linear equilibrium between the two phases ($C_\mu = K \cdot C$) over the pressure range within which the kinetic experiments are conducted, the solution for the pressure response in the adsorber is given by (Do, 1995)

$$P = \frac{(\dot{N}t)R_gT/V}{(1+\beta)} + \frac{\beta}{(1+\beta)^2}\frac{\dot{N}R_gT}{V}\frac{R^2}{(s+1)(s+3)D_{\text{app}}} - 2(1+s)\beta\left[\left(\frac{\dot{N}R_gT}{V}\right)\left(\frac{R^2}{D_{\text{app}}}\right)\right] \times \sum_{n=0}^{\infty}\frac{\exp\left[-\lambda_n^2\left(D_{\text{app}}t/R^2\right)\right]}{\lambda_n^2\left[(1+s)^2\beta^2 + (1+s)^2\beta + \lambda_n^2\right]}, \tag{3}$$

where R is half length of the slab particle, R_g is the gas constant, and T is the temperature of the system. The equilibrium parameter β and the apparent diffusivity D_{app} are defined below:

$$\beta = \frac{V_{\text{app}}}{V} = \left(\frac{m_p}{\rho_p}\right)\left[\frac{\epsilon_m + (1-\epsilon_m)K}{V}\right] \tag{4}$$

$$D_{\text{app}} = \frac{\epsilon_m D_p + (1-\epsilon_m)KD_s}{\epsilon_m + (1-\epsilon_m)K}, \tag{5}$$

with D_p and D_s being pore and surface diffusivities, respectively. The eigenvalues λ are obtained from the following transcendental equation:

$$\beta\tan(\lambda) + \lambda = 0.$$

The pressure response, as given in Eq. 3, increases with time, and when time is sufficiently great, it will reach the linear asymptote described by the first two terms in that equation. This equation will be used in our work to determine the kinetics parameters, and we adopt two approaches in order to accomplish this. In one approach we use the full transient solution and match it with the experimental data to obtain the necessary parameters, while in the second approach only the linear asymptote is used for the same purpose. We briefly describe these two approaches below.

Approach 1

Although it is very convenient to obtain the parameters by using the linear part of the dynamics curve, matching the full transient equation to the experimental data was found to be more reliable. In our kinetic experiments, we used three particle sizes, three temperatures, and a range of molar flow rates (2 to 12×10^{-9} mol/s). The runs were terminated when the pressure response reached a linear asymptote, and for the adsorbates studied here, the termination pressure was about 5 torr, at which the adsorption isotherm is still linear, allowing the application of the linear mass-transfer model. The kinetic data of pressure vs. time were analyzed using Eq. 3 to extract the kinetic parameter D_{app}. The parameter β in this equation was determined from the equilibrium experiment.

Approach 2

The second approach in the parameter determination is to use the linear asymptote of the pressure response vs. time. This linear asymptote can be utilized to determine not only the kinetic parameter D_{app} but also the equilibrium parameter K. The linear asymptote of the pressure response vs. time can be described by the first two terms on the righthand side of Eq. 3, and it has the following slope and intercept:

$$\text{Slope} = \frac{\dot{N}R_gT/V}{(1+\beta)} \tag{6a}$$

$$\text{Intercept} = \frac{\beta}{(1+\beta)^2}\frac{\dot{N}R_gT}{V}\frac{R^2}{(s+1)(s+3)D_{\text{app}}}. \tag{6b}$$

We note that the slope (Eq. 6a) contains the equilibrium parameter β (related to the Henry constant K according to Eq. 4). Thus, if we do not have information on the Henry constant, it can be determined from the slope of the linear asymptote. However, if we have the Henry constant from an independent equilibrium experiment, it can be used to our advantage to check the slope of the linear asymptote to ensure that the correct linear asymptote has been achieved experimentally. Thus, knowing the equilibrium parameter β from either the Henry constant or from the slope of the linear asymptote, we can calculate the kinetic parameter D_{app} from the intercept (Eq. 6b).

Results and Discussion

Adsorption kinetics of methane, ethane, propane, and butane on Ajax AC particles have been conducted in a semibatch CMF adsorber. Equilibrium experiments were carried out at different temperatures to determine the adsorption isotherms from which the adsorption affinity and the heat of adsorption can be calculated and subsequently used in the analysis of kinetic data.

A series of light hydrocarbons were selected as the model adsorbates for testing the constant molar flow method for the reliability of the technique in dealing with adsorbates ranging from weak to strong, and from small to large molecules. How strong or weak an adsorbate is will affect the adsorption capacity, while the size of the molecule will affect the mobility of adsorbed species inside the particle.

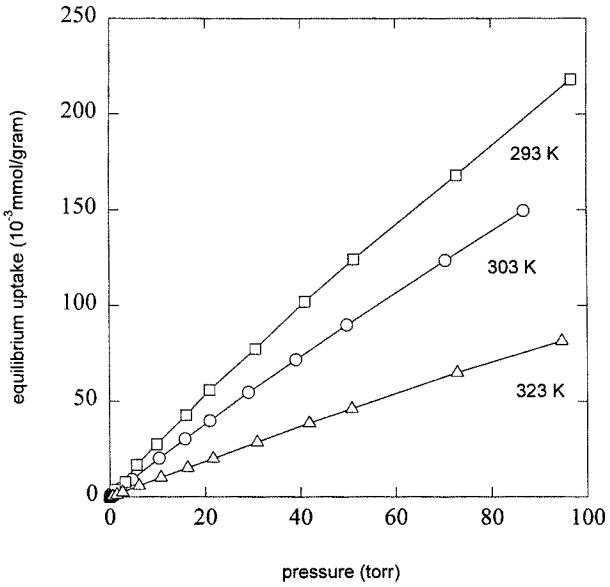

Figure 2. Adsorption isotherms of methane on Ajax AC at various temperatures.

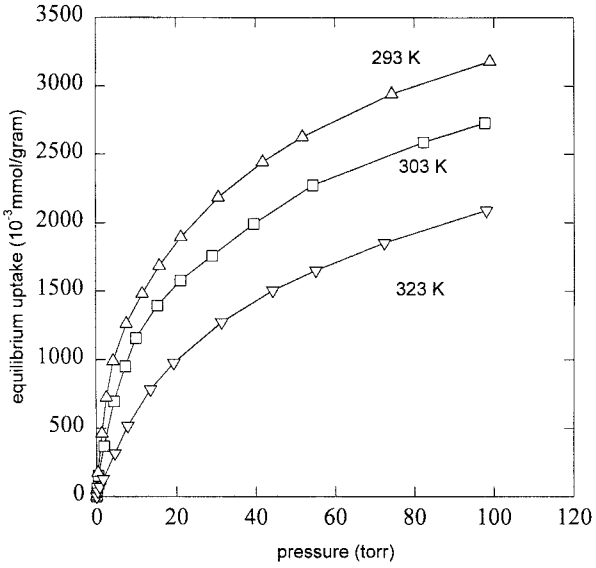

Figure 4. Adsorption isotherms of propane on Ajax AC at various temperatures.

Equilibrium isotherms

The adsorption isotherms were measured by the volumetric method using the same experimental rig shown in Figure 1. The data obtained were then analyzed for the Henry constant, which is the slope of the isotherm at zero loading. We also determined the range of the Henry law region, so that the pressure beyond which the isotherm becomes nonlinear was set as the maximum for the pressure evolution in the kinetic measurement. This was because the theoretical analysis of kinetics is based on linear isotherm assumption. Adsorption isotherms of methane, ethane, and propane on Ajax AC in the pressure range of 0–100 torr are shown in Figures 2, 3, and 4, respectively. For each species three temperatures, 293, 303, and 323 K, were used. In Figures 2 and 3 we see that the adsorption isotherms of methane and ethane are linear up to a pressure of about 100 and 10 torr, respectively, whereas for propane, the linear partition between the gas phase and the adsorbed phase occurs up to about 5 torr (Figure 4). Since all of our kinetics experiments were conducted within 5 torr, the linear analysis for mass transfer is applicable.

The values of the Henry constant at three different temperatures are summarized in Table 2 and shown graphically in Figure 5 as plots of $\ln(K)$ vs. $(1/T)$. The affinity of the adsorbate toward the adsorbent increase with the carbon number, as one would physically expect. The heats of adsorption as calculated from the van't Hoff equation are also included in Table 2. Like the adsorption affinity, the heat of

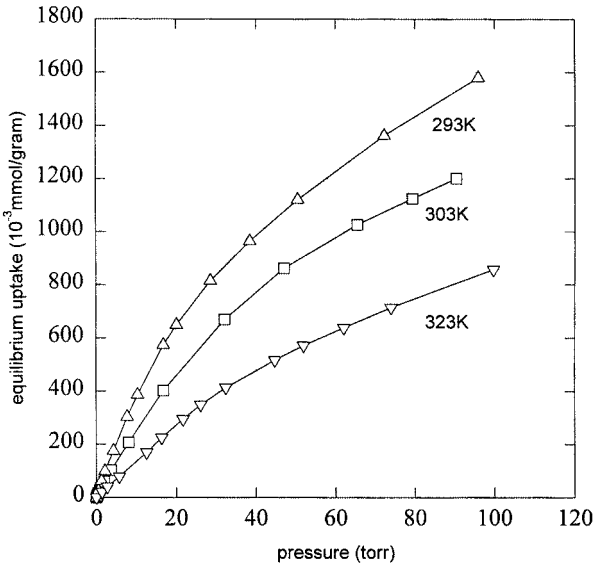

Figure 3. Adsorption isotherms of ethane on Ajax AC at various temperatures.

Table 2. Heat of Adsorption and Henry Constants for Methane, Ethane, Propane, *n*-Butane in Ajax Activated Carbon

Adsorbate	Temp. (K)	Henry Const., K^*	ΔH (kcal/mol)
Methane	293	44	5.9
	303	39	
	323	20	
Ethane	293	772	6.2
	303	524	
	323	285	
Propane	293	5,742	8.4
	303	3,269	
	323	1,490	
n-Butane	293	10,760	10.1
	303	6,550	
	323	2,130	

*Dimensionless, $K = (K_P \rho_p RT)/(1-\epsilon)$; K_P unit = gmol/(gram × torr).

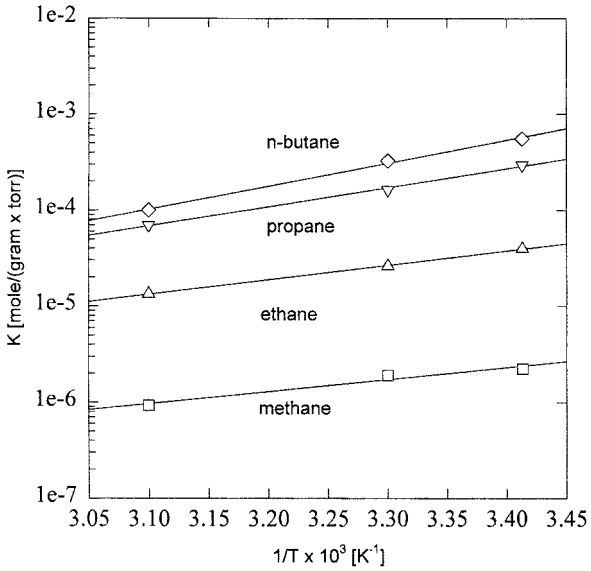

Figure 5. Temperature dependence of Henry constant for methane, ethane, propane, and butane.

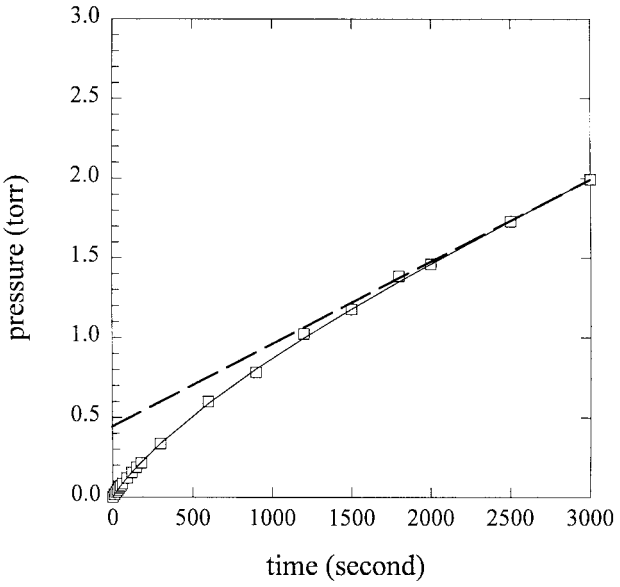

Figure 6. Typical pressure response vs. time.

adsorption also increases with the carbon number, while the heat of adsorption of butane is almost twice as high as that for methane.

Sorption kinetics

Sorption kinetics data at three temperatures (293, 303 and 323 K), three molar supply rates, and three particle sizes (L = 0.5, 0.75 and 1 cm) were collected using the semibatch CMF adsorption apparatus. Detailed operation procedures have been provided in the experimental section.

The apparent diffusivities of methane, ethane, and propane in Ajax AC were found to be independent of particle size (supporting the diffusion mechanism assumed in the model). These values are tabulated in Table 3 for the three temperatures used in this study.

A typical plot of the pressure response vs. time is shown in Figure 6, where two regions can be observed. In the first region, the pressure response exhibits a concave shape, and the system pressure approaches a linear asymptote at the end of the first region. In the second region, we observe a linear asymptote that is the result of the balance between the molar flow rate introduced into the adsorber and the rate of adsorption. Figure 7 shows the effect of two different sizes of slab-activated carbon for the same molar supply rate. The pressure-response curve for the longer slab takes a longer time to reach the linear asymptote as one would physically expect. It also can be seen from the figure that the two linear asymptotes corresponding to the two slab particle sizes have the same slope, and their intercepts are proportional to the square of particle size, confirming the theoretical slope and intercept as given in Eqs. 6.

Figure 8 shows the experimental pressure responses and the corresponding linear asymptotes for propane adsorption, at 303 K for the 0.5-cm slab of activated-carbon particle with

Table 3. Summary of Dynamic Parameters (D_{app}) of Methane, Ethane, Propane, and n-Butane in Ajax Activated-Carbon Particles at 303 K

Adsorbate	Henry Const., K*	β	D_{app} (cm^2/s)
Methane	39	0.1075	8.0×10^{-3}
Ethane	524	0.7143	4.73×10^{-4}
Propane	3,269	2.2264	6.86×10^{-5}
n-Butane	6,550	4.4606	2.63×10^{-5}

*See footnote to Table 2.

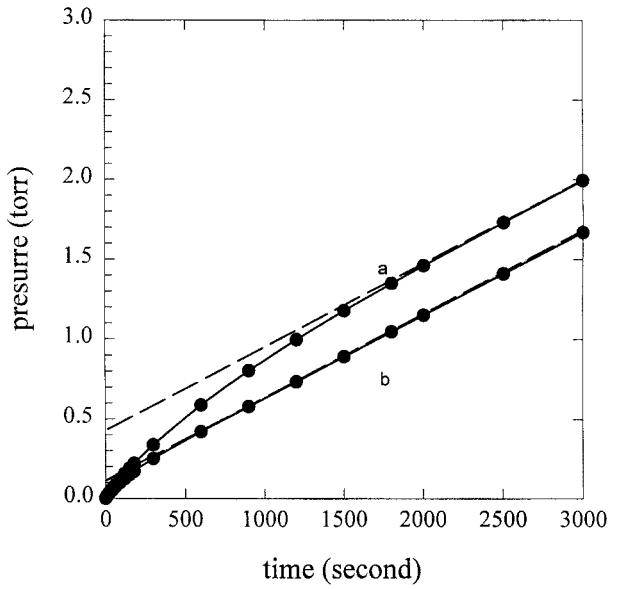

Figure 7. Pressure response for propane at 303 K on slab-shaped activated-carbon particles of two different sizes, L = 1.0 cm and 0.5 cm.

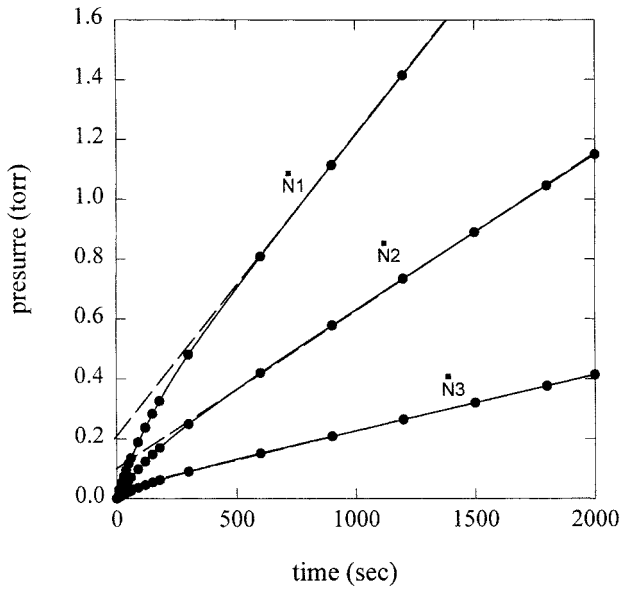

Figure 8. Pressure response for propane at 303 K on slab-shaped activated-carbon particles (L = 0.5 cm) at three different flow rates.

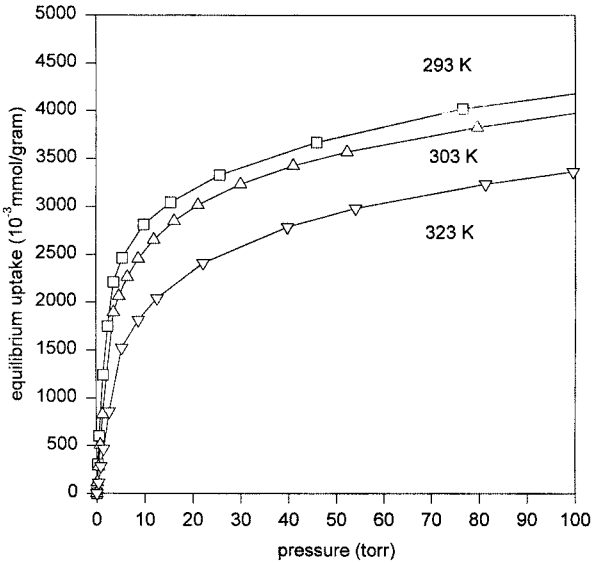

Figure 9. Adsorption isotherms of *n*-butane on Ajax AC at various temperatures.

three values of molar flow rate (2.15, 6.25, and 12.05×10^{-9} mol/s). The slope and the intercept of the linear asymptote, as given in Eqs. 6a and 6b, are proportional to the molar supply rate of the adsorbates. Thus to validate the theory, we take the ratio of the slope to the intercept for different molar flow rates to check whether it is in fact independent of flow rate:

$$\frac{\text{Slope}}{\text{Intercept}} = \frac{(1+\beta)}{\beta}\,\frac{(s+1)(s+3)D_{\text{app}}}{R^2}. \qquad (7)$$

Our experimental data indeed agree with this, confirming the validity of the model. The independence of the preceding ratio vs. the molar flow rate also indicates that the linear asymptote has been correctly determined. The value of the slope/intercept ratio of linear asymptotes of the pressure-response curves is summarized in Table 4 for propane, where we see that the slope/intercept ratio is almost a constant.

As we discussed in the previous section, the linear asymptote of the pressure response vs. time can be described by the first two terms of Eq. 3, and it can be utilized to determine the relevant equilibrium and kinetic parameters. From the slope, we can obtain the equilibrium parameter, β, and then the dynamic parameter, D_{app}, can be obtained from the intercept. This is an obvious advantage of this method, especially when we have many samples to analyze for their kinetic parameters. Using this approach, we present the equilibrium parameters, β, obtained for all hydrocarbons studied in Table 3. The mobility of the hydrocarbon series (from C_1 to C_4) represented by the value of the diffusivity in each adsorbent shown in the table can indicate how selective the adsorbent is with those molecules.

Table 4. Apparent Diffusivity of Propane on Ajax Activated Carbon at 303 K at Various Flow Rates

Molar Flow Rate (mol/s)	Slope	Intercept	Slope/Intercept	D_{app} (cm^2/s)
2.15×10^{-9}	1.8×10^{-4}	0.04	0.0045	6.89×10^{-5}
6.25×10^{-9}	5.2×10^{-4}	0.12	0.0043	6.83×10^{-5}
12.05×10^{-9}	10.0×10^{-4}	0.21	0.0046	6.91×10^{-5}

Sorption of n-Butane. Adsorption equilibria of *n*-butane on Ajax AC at three temperatures (293, 303 and 323 K) is presented in Figure 9, and the values of Henry constant are presented in Table 5. It was observed that *n*-butane is the strongest adsorbing species among the four hydrocarbons investigated. We also note that the linear portion of the isotherm in *n*-butane adsorption could not be detected clearly within the range of pressure employed for methane, ethane, and propane (0–5 torr). The dynamics measurement of *n*-butane was therefore terminated at about $p = 1$ torr, where the approximate Henry law condition up to this pressure is still acceptable. The indication of nonlinearity shown by *n*-butane suggests that the linear model may not be applicable for hydrocarbons having higher carbon number. Therefore, to determine the D_{app} of gases or vapors that are stronger than *n*-butane, it is necessary to develop a nonlinear model. This will be the subject to our future study when we deal with stronger adsorbed molecules such as aromatics hydrocarbons.

Activation energy of the surface diffusion

After extracting the apparent diffusivities from the pressure-response curve of the sorption kinetics experiment, we use Eq. 5 to determine the surface diffusivity. This is done by using the following equation to calculate the pore diffusivity:

$$D_p = \frac{D_K}{\tau} \qquad (8)$$

Table 5. Apparent Diffusivity, Surface Diffusivity, and Activation Energy for Surface Diffusion for Methane, Ethane, Propane, and *n*-Butane

Temp. (K)	Henry Const., K^*	D_{app} (cm^2/s)	D_s (cm^2/s)	E (kcal/mol)
Methane				
293	44	6.98×10^{-3}	1.30×10^{-4}	2.8
303	39	8.0×10^{-3}	1.52×10^{-4}	
323	20	15.83×10^{-3}	2.02×10^{-4}	
Ethane				
293	772	6.98×10^{-4}	3.50×10^{-5}	3.2
303	524	6.98×10^{-4}	4.21×10^{-5}	
323	285	6.98×10^{-4}	5.86×10^{-5}	
Propane				
293	5,742	4.06×10^{-4}	0.86×10^{-5}	5.1
303	3,269	6.86×10^{-4}	1.15×10^{-5}	
323	1,490	14.86×10^{-4}	1.94×10^{-5}	
n-Butane				
293	10,760	1.59×10^{-5}	1.025×10^{-6}	6.72
303	6,550	2.63×10^{-5}	1.501×10^{-6}	
323	2,130	8.17×10^{-5}	2.994×10^{-6}	

*Dimensionless, $K = (K_P \rho_p RT)/(1-\epsilon)$.

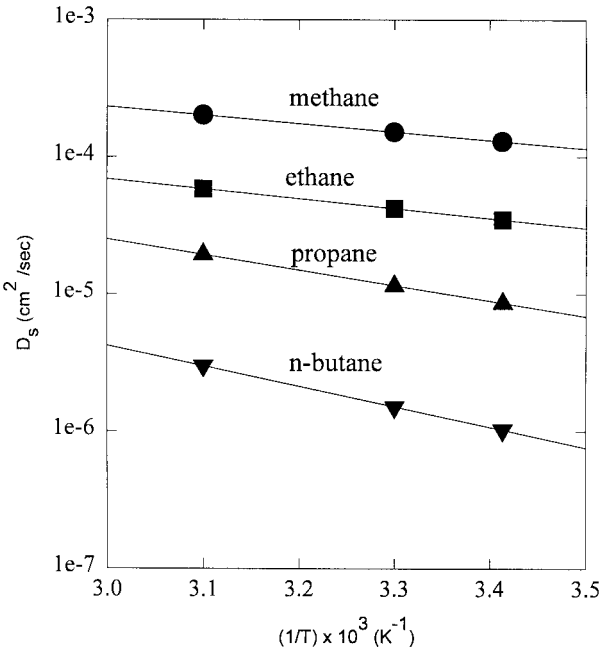

Figure 10. Temperature dependence of surface diffusivity (D_s) for methane, ethane, propane, and *n*-butane.

where τ is the macropore tortuosity factor of the porous material, and D_K is the Knudsen diffusivity, which can be estimated from the kinetic theory of gases. For a gas of molecular weight M at T kelvin diffusing along the pore with a μ cm mean radius, the value of D_K (cm^2/s) is

$$D_K = 9{,}700\mu\left(\frac{T}{M}\right)^{1/2}. \qquad (9)$$

The mean macropore size and the tortuosity factor (0.8 μm and 4.9, respectively) were obtained by independent means. Thus knowing the pore diffusivity, the surface diffusivity can be calculated (Table 5). The values of surface diffusivity of ethane and propane obtained by this technique are close to the values determined by the DAB method (Mayfield and Do, 1991; Do et al., 1991).

Activation energy of the surface diffusion for each gas in the Ajax AC were determined by an Arrhenius plot, as shown in Figure 10, where the surface diffusivity D_s for different T were plotted in logarithmic scale vs. $1/T$. By a least-squares fit ($D_s = D_0 \exp[-E/R_g T]$), the activation energy for surface diffusion was determined from the data; the values are presented in Table 5. These activation energies for four paraffins—methane, ethane, propane, and *n*-butane—are plotted in Figure 11a vs. the molecular weight. The heat of adsorption at zero loading is also plotted for comparison. We see that the activation energy for surface diffusion is less than the heat of adsorption, and they both increase with the molecular weight, since one would expect that the species with a higher boiling point would have a higher heat of adsorption. The ratio of the activation energy for surface diffusion to the heat of adsorption is plotted against the molecular weight in Figure 11b. We note that this ratio increases from 0.45 to 0.65 as we move from methane to *n*-butane. These values are comparable to those reported by Chihara et al. (1978) and Gilliland et al. (1974). What this seems to indicate is that because the molecule is larger, the energy barrier is approaching the heat of adsorption. This supports the concept of surface diffusion proposed by Do (1996) for the diffusion of adsorbed species in activated carbon. In this model, it was assumed that activated carbon is composed of units of graphitic layers. Molecules enter the unit, diffuse within the graphitic units, and then evaporate from the other end of the unit. Activation energy within the unit could be estimated from the energy interaction between the adsorbate and the surface atom (Rao et al., 1985). The process of entering the pore and leaving the pore would have an energy equivalent to that of adsorption. Thus the observed ratio of activation energy for surface diffusion to heat of adsorption approaching unity indicates that the processes of entering and evaporating control the transport. This seems reasonable because one would expect that the penetration of the larger molecule into the micropore network would be more difficult than for the smaller molecules. This difficulty of entering the micropores will reach the stage where molecules larger than the pore size are kept from entering the pore. Thus the mechanism for transporting molecules in activated carbon appears to be composed of the following processes:

1. Pore diffusion along the mesopore network
2. Finite mass exchange from the fluid phase to the adsorbed phase (micropore)
3. Surface diffusion along the adsorbed phase.

For small molecules, the second process is usually fast compared to the others, so the overall kinetics is dictated by the dual-diffusion process. On the other hand, when the molecule is larger, the three processes control the transport into the particle. If the molecule grows even larger, the overall kinetics is dictated by the second process, that is, the ability of the

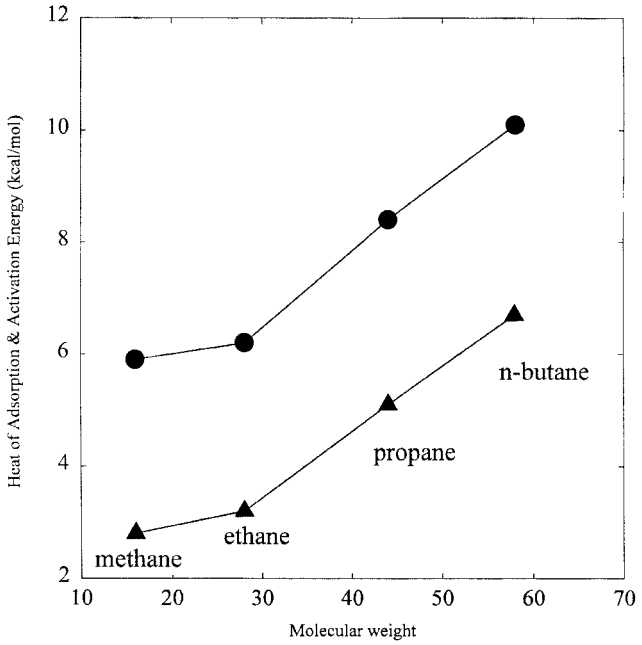

Figure 11a. Activation energy for diffusion and isosteric heat of adsorption vs. molecular weight.

molecule to enter the pore. This is the case one would observe for a carbon molecular sieve. These processes have been considered in a comprehensive mathematical model proposed by Do and Wang (1998a,b).

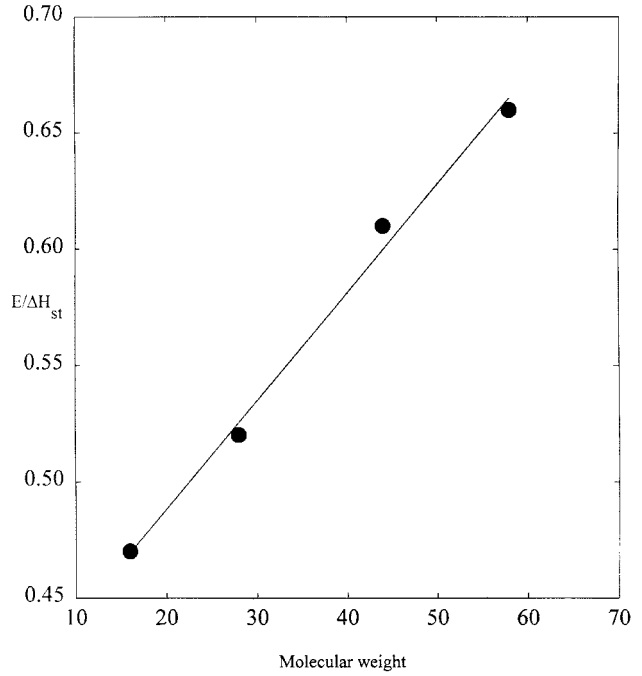

Figure 11b. Ratio of the activation energy for diffusion to the isosteric heat of adsorption vs. molecular weight.

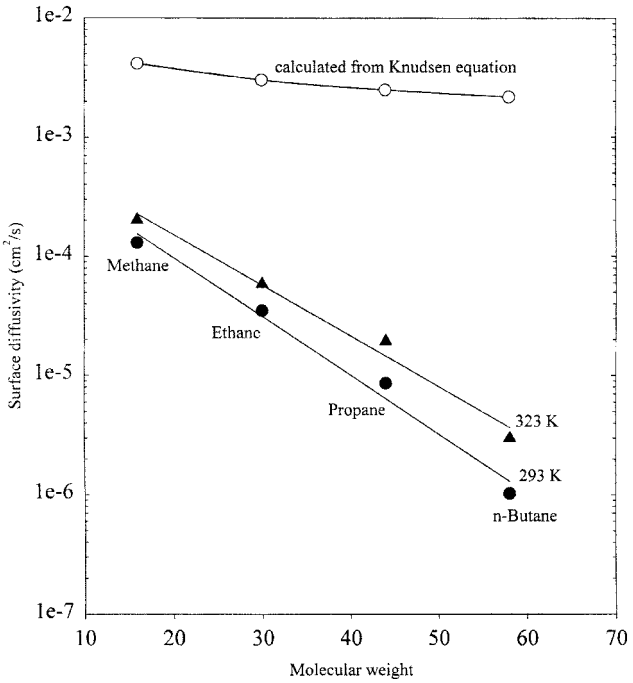

Figure 12. Surface diffusivities vs. molecular weight.

To investigate the variation of the surface diffusivity vs. the molecular weight, we plot this relationship in a semilog plot (Figure 12). We observe a linear relationship, that is, the surface diffusivity takes the following form at 293 K:

$$D_s = (1\times 10^{-3})10^{-MW/20}\ \text{cm}^2/\text{s}. \qquad (10)$$

By assuming a micropore size of 1 nm, we calculate the Knudsen diffusivity and present the results in Figure 12. Here we see that the experimental diffusivities are much lower than those calculated from the Knudsen equation, suggesting that the flow in the micropore is not of Knudsen origin, but rather an activated process with an energy of less than the heat of adsorption. For the four paraffins investigated here, this fraction is of the order of 0.5.

Conclusions

In this article, we have presented a study of the adsorption of a light hydrocarbon series (methane, ethane, propane, and *n*-butane) on activated carbon by a semibatch CMF method. The method has shown great promise for the study of the kinetics of gases and vapors in porous media. For the light paraffins studied here, the mobility is found to decrease with an increase in the carbon number, and the surface diffusivity was found to be on the order of 10^{-5} cm^2/s, which is on the same order of magnitude as those obtained by other methods.

Acknowledgment

This project is funded by the Australian Research Council.

Notation

E = activation energy for surface diffusion (cal/mol)
k_a, k_d = rate constants for adsorption and desorption
K_P = Henry constant (mol/g/torr), defined in Table 2
m_p = mass of particle (g)
M = molecular weight (g/mol)
P = pressure (torr)
Q = heat of adsorption (cal/mol)
r = radial distance in the particle, cm
R = particle radius for cylinder (cm)
s = particle shape factor
t = time (s)
V_μ = volume of the adsorbed phase, cm^3
x = nondimensional distance in the particle
ϵ_m = porosity of the particle
μ = pore radius (cm)
ρ_p = particle density (g/cm^3)

Literature Cited

Chihara, K., M. Suzuki, and K. Kawazoe, ''Adsorption Rate on Molecular Sieving Carbon by Chromatography,'' *AIChE J.*, **24**, 237 (1978).

Do, D. D., ''Dynamics of a Semi-Batch Adsorber with Constant Molar Supply Rate: A Method for Studying Adsorption Rate of Pure Gas,'' *Chem. Eng. Sci.*, **50**, 549 (1995).

Do, D. D., ''A Model for Surface Diffusion on Ethane and Propane in Activated Carbon,'' *Chem. Eng. Sci.*, **51**, 4145 (1996).

Do, D. D., X. Hu, and P. Mayfield, ''Multicomponent Adsorption of Ethane, *n*-Butane, and *n*-Pentane in Activated Carbon,'' *Gas Sep. Purif.*, **5**, 35 (1991).

Do, D. D., and K. Wang, ''Dual Diffusion and Finite Mass Exchange Model for Adsorption Kinetics in Activated Carbon,'' *AIChE J.*, **44**, 68 (1998a).

Do, D. D., and K. Wang, ''A New Model for the Description of Sorption Kinetics in Heterogeneous Activated Carbon,'' *Carbon*, **36**, 1539 (1998b).

Gilliland, E. R., R. F. Baddour, G. P. Perkinson, and K. J. Sladek, ''Diffusion on Surfaces. I. Effect of Concentration on the Diffusivity of Physically Adsorbed Gases,'' *Ind. Eng. Chem. Fundam.*, **13**, 95 (1974).

Gray, P. G., and D. D. Do, ''Dynamics of Carbon Dioxide Sorption on Activated Carbon Particles,'' *AIChE J.*, **37**, 1027 (1991).

Mayfield, P. L. J., and D. D. Do, ''Measurement of the Single Component Adsorption Kinetics of Ethane, Butane and Pentane onto Activated Carbon Using a Differential Adsorption Bed,'' *Ind. Eng. Chem. Res.*, **30**, 1262 (1991).

Prasetyo, I., and D. D. Do, ''Adsorption Rate of Methane and Carbon Dioxide on Activated Carbon by the Semi-Batch Constant Molar Flow Rate Method,'' *Chem. Eng. Sci.*, **53**, 3459 (1998).

Rao, M. B., R. G. Jenkins, and W. A. Steele, ''Potential Functions for Diffusive Motion in Carbon Molecular Sieves,'' *Langmuir*, **1**, 137 (1985).

Manuscript received Nov. 19, 1998, and revision received May 10, 1999.